The error in B values and corrected values are described in detail elsewhere (*1*). The error in B values, which was due to a typographical error in a numerical program used earlier (*8*), amounted to about 7% in the G region of interest in withdrawal. Comparison of the new B values with equivalent values obtained independently by another numerical technique (*2*) confirmed that the new values are accurate to at least four significant figures.

The error due to the previous use of the improper range of G has been discussed and minimized, as described elsewhere (*5*). The previous range used, namely G of 0.03 to 3 (*8*), was replaced by choosing the G range so as to minimize the error in curvature in Equation (3). Comparing the magnitude of each term in Equation (3), using $\alpha = 2.4$ and $\beta = 0.85$ as reasonable estimates, indicated that the region for which the ϕ correlation should be most precise occurs at G_0 of 1 to 30 and higher. A log-log plot of ϕ vs. G in this region indicated a β of unity and $\alpha = 3.36$. Thus the more accurate description of top curvature for a static menisci on a cylinder is (*5*)

$$C_S \doteq \frac{3.36G}{1 + 3.36G} + \frac{1}{2G} \qquad (7)$$

Use of the new α and β values corrects the previous errors in Equation (4). As a check, C_S values obtained using empirical Equation (7) were compared with theoretical values of four to five place accuracy for a range of G (0.003 to 30). The new curvature values from Equation (7) were found to be accurate to within 0.5% for all G and, furthermore, to be accurate to within 0.1% for all $G < 0.02$ and all $G > 2$. The largest differences of 0.3 to 0.5% were noted at G from 0.07 to 0.7.

THE NEW DYNAMIC CURVATURE EXPRESSION [EQUATION (8)]

Using Equation (7) and the static to withdrawal transformation described above, the curvature for the top of a withdrawal meniscus is now given as

$$C_m \doteq \frac{3.36(SG)}{1 + 3.36(SG)} + \frac{1}{2(SG)} \qquad (8)$$

Equation (8) is a new equation.

Comparison of C_m of Equation (8) with $C_m{}^*$ of Equation (5) indicates that the old $C_m{}^*$ value has errors of 2 to 6% in the GS range of 0.3 to 3 and errors of about 6% in the GS range of 3 to 30.

Use of the C_m of Equation (8) is recommended in all available continuous withdrawal theories for cylinders (*6*), including Equation (6) for Newtonian fluids (*7, 10*), the special-case Newtonian theories for low speeds (*9*), and the theory for non-Newtonian fluids (*4*). The effect of the improved precision should be most apparent at larger radii (larger G) and higher speeds (thicker films and larger S) or both (larger GS).

ACKNOWLEDGMENT

This work was supported by NSF Grant GK-1206.

LITERATURE CITED

1. Hildebrand, R. E., M. A. Hildebrand, and J. A. Tallmadge, in preparation.
2. Huh, Chun, and L. E. Scriven, *J. Colloid Interface Sci.*, **30**, 323 (1969).
3. Rajani, G. R., MS thesis (Chem Eng.), Drexel Inst. Tech., Philadelphia, Pa. (June, 1968).
4. Tallmadge, J. A., *AIChE J.*, **14**, 837 (1968).
5. ———, in preparation.
6. Tallmadge, J. A., and Chaim Gutfinger, *Ind. Eng. Chem.*, **59**, No. 11, 18 (1967). Errata, **60**, No. 2, 74 (1968).
7. Tallmadge, J. A., and D. A. White, *Ind. Eng. Chem. Process Design Develop. Quart.*, **7**, 503 (1968).
8. White, D. A., and J. A. Tallmadge, *J. Fluid Mech.*, **23**, 325 (1965).
9. ———, *AIChE J.*, **12**, 333 (1966).
10. *Ibid.*, **13**, 745 (1967).

Area-Free Mass Transfer Coefficients for Liquid Extraction in a Continuously Worked Mixer

R. B. KEEY and J. B. GLEN

University of Canterbury, Christchurch, New Zealand

Most reported data for continuous-phase mass transfer in agitated extraction vessels are expressed in terms of $K_c a$, the mass transfer coefficient per unit volume. Recently Schindler and Treybal (*17*) report some area-free coefficients for the continuous extraction of water-saturated ethyl acetate with water itself. The object of this paper is to describe other data for area-free coefficients that pertain to continuously worked extractors of similar design. The system, however, differs in that it is ternary: a solute is extracted from the dispersed phase into the continuous phase, both phases being presaturated with respect to the other nonsolute.

THEORY

In an earlier paper (*9*), we derived an expression for the continuous-phase mass-transfer coefficients by using Lin and coworkers' ideas (*12*) on turbulence damping. Near a mobile surface, where the energy loss through dissipation in the continuous-phase boundary layer may be less than near a rigid surface, Piterskikh's relationship may hold:

$$\nu_{\text{turb.}} = b\ \nu_c (y/\delta_0)^2 \qquad (1)$$

where b is a coefficient of order 0.01 (*11*). A parallel argument leads to

$$K_c = \sqrt{C_{DF}}\ U\ N_{Sc}{}^{-1/2} \qquad (2)$$

in which C_{DF} is the drag coefficient for the mobile drop and U is the relative velocity between the drop and the continuous phase. This slip velocity is widely fluctuating due to the turbulence created by the impeller. An expression for the maximum slip velocity has been derived by Levich (*11*) when the motion of the particle can be described in terms of self-preserving range of turbulence frequencies. Levich finds, when gravitational and supplemental reaction terms are neglected and entrainment is nearly complete, that

J. B. Glen is with ICIANZ, Melbourne, Victoria, Australia.

$$U_{max} \approx \frac{\Delta\rho}{\rho_D} d_p \left(\frac{\epsilon}{\rho_c \nu_c}\right)^{1/2} \quad (3)$$

Further, the dissipation ϵ is governed only by those quantities that characterize the largest (and energy-containing) eddies: the density, ρ_c, the integral scale ($\sim d_I$) and the velocity fluctuation ($\sim Nd_I$) (10). So

$$\epsilon \sim \rho_c (Nd_I)^3/d_I \quad (4)$$

The time-smoothed mass transfer coefficient $\overline{K}_c$ will be determined by the root-mean-square value of the slip velocity U_{RMS}. Roughly, $U_{RMS} \sim U_{max}$ so that Equations (2), (3), (4) may be combined to yield

$$N_{Sh} = \frac{\overline{K}_c d_I}{\mathcal{D}} \sim \sqrt{C_{DF}}\, N_{ReI}^{3/2}\, N_{Sc}^{1/2} \quad (5)$$

in which the undetermined coefficient is entirely dimensionless and contains the parameters $\Delta\rho/\rho_D$ and (dp/d_I). We present Equation (5) merely to show the functional dependence of the Sherwood number on the impeller Reynolds number. Normally it is assumed that the drag coefficient C_{DF} is independent of Reynolds number over the flow region of interest. However, the particle Reynolds number is at least 100 times smaller than the impeller Reynolds number, even when the particles are barely entrained. For an impeller Reynolds number range between 10^4 and 10^5, then, the drag coefficient will be a weak function of the Reynolds number:

$$C_{DF} \sim N_{ReI}^{-1/4} \quad (6)$$

Insertion of this proportionality into Equation (5) yields

$$N_{Sh} \sim N_{ReI}^{-11/8}\, N_{Sc}^{1/2} \quad (7)$$

EXPERIMENTAL EQUIPMENT

The closed mixing vessels employed were similar in design to the vessel used by Schindler and Treybal (Figure 1 of reference *17*). The liquid inlets were concentric at the base, with an overflow outlet concentric to the impeller shaft. Four baffles of width 1/8th of the vessel diameter were employed and outset from the wall by 1.6 mm. to avoid stagnant zones. Each impeller was mounted at the vessel center and consisted of a six-bladed paddle. Table 1 details the geometries employed.

EXPERIMENTAL PROCEDURE

The organic, dispersed phase was iso-octane of 99.9% purity. The solute was doubly steam-distilled *o*-nitrophenol (m.p. 45 ± 0.2°C.). To avoid dissociation of the solute, the continuous phase, soft tapwater, was acidified to *p*H 3.5 ± 0.3; total dissolved solids in the water were less than 0.01g./100g. The feed streams were continuously pumped to the concentric inlet, and continuously withdrawn by overflow to the extract settler. The system was capable of closed-loop operation.

The droplets were photographed on emerging from the vessel through a microscope-slide window in the outlet, Figure 1. The negatives were projected to estimate the drop-size spectrum by counting drops in progressive size increments of < 3, 3 to 6, 6 to 10, 10 to 15, 15 to 25, 25 to 40, and > 40 mm. The method is useful only for small volume fractions of dispersed phase; φ_D was never greater than 0.112 in our tests. For the finer dispersions, only about 10% of the total negative area was selected for counting, the criterion being the sharpness of the picture. About 2,000 drops were counted for each dispersion and about eight negatives were required to achieve this number.

To measure the outgoing concentration of solute, a sample tube from the top of each vessel was led to a settling vessel. The residence time in the transfer line was found by watching the finest droplets entrained in the aqueous phase; this transfer time was between 2 and 3 sec. A fraction of the settled aqueous phase was withdrawn at a rate of about 2 cc./sec. through a light-absorption cell. A Hilger Watts continuous absorptiometer, H954, was modified by introducing an 0.2 kw. mercury-arc source, which demanded modified optical paths and a cooling fan. Heat filters and Wood's glass filters were placed in the reference and analysis paths to allow a light transmittance of a wave-length near 3,500 Å. The iso-octane and water do not absorb light of this wavelength, and the dissociated *o*-nitrophenol has an absorption peak of about 5,800 Å (3). Because of the slow drift of the spectrophotometer output, the meter was zeroed with solute-free material before each run. The concentration of the incoming extract phase was determined by extracting four samples into potassium hydroxide solution (*p*H > 12); the samples were then diluted, acidified to *p*H 3.5 and analyzed by a Hilger ultra-violet spectrophotometer. The concentration of *o*-nitrophenol into the iso-octane phase before extraction was maintained at about 0.004g. *o*-nitrophenol/g. solvent.

At the end of each run, an aqueous sample of about 50 cc. was collected for a check analysis with a Beckmann DK2 spectrophotometer. This analysis agreed with in-process analyses to within ± 4% unless inadvertent contamination had occurred. The scale-reading error for the two concentration-analysis methods is ± 3% for an extraction efficiency of 0.5. However, the error in the mass transfer coefficient is ± 6%, as the outlet concentration of the

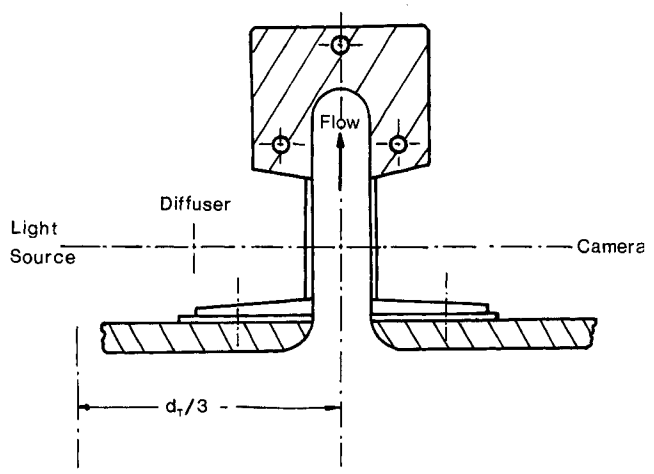

Fig. 1. Dispersion viewing window; vertical section.

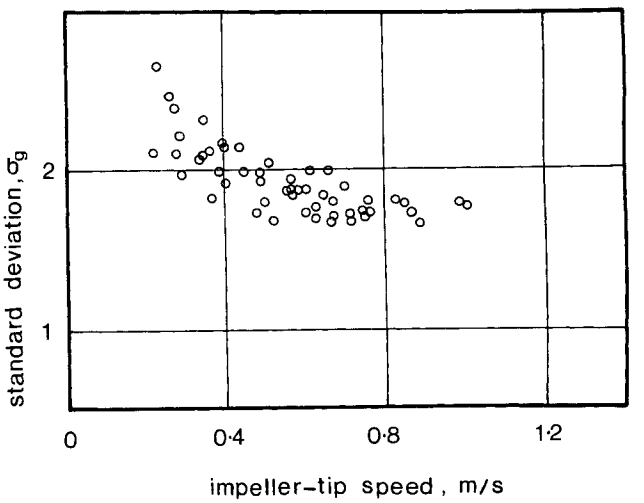

Fig. 2. Standard deviation of drop-size spectrum as a function of power dissipated by the agitator.

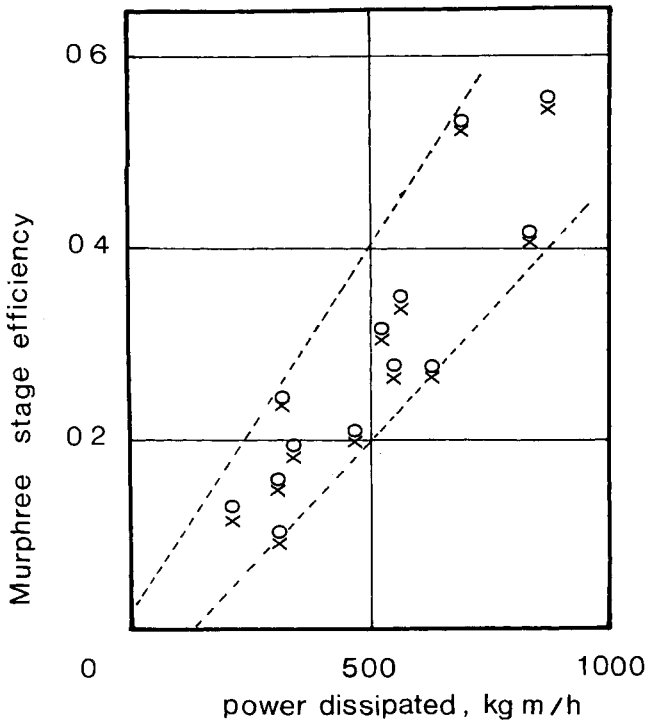

Fig. 3. Murphree stage efficiencies of mixer, at low power inputs as a function of the power dissipated by the agitator; points X uncorrected, points 0 corrected for end effects.

aqueous phase is used to estimate the total solute transferred as well as the driving force. The error rises as the efficiency approaches 0 or 1; at an efficiency of 0.85, the error becomes ± 12%.

The flow of each phase was measured by a rotameter. Physical-property data are recorded elsewhere (*6*).

RESULTS

The system is continuous-phase controlled as $c_D/c_C^* >> 1$. The overall mass transfer coefficient may thus be calculated from the mass balance

$$Q_C\ c_{C_2} = \overline{K}_C\ \overline{a}_i\ V_T\ \Delta c_m \qquad c_{C_1} \simeq 0 \tag{8}$$

The mean interfacial area per unit volume, $\overline{a}_i$, is computed from the mean diameter of the dispersion, $\Sigma nd^3/\Sigma nd^2$, obtained from photographic analyses of the outlet. A diameter-frequency plot for each run showed the particle sizes to have a logarithmic-normal distribution (*6*). Drop diameters greater than d_{98} tended to scatter, and those less than d_{30} occurred more frequently. A smoothed frequency distribution was obtained by assuming a logarithmic-normal distribution of particle sizes, and so an estimate of the volume-surface drop diameter could be made:

$$\log\ d_{vs} = \log\ d_{50} + 5.757\ \log^2\ \sigma_g \tag{9}$$

A plot of the standard deviation σ_g against impeller-tip speed is given in Figure 2. The narrowing range of droplet diameters with increasing impeller speed is expected from considerations of stable drop sizes.

This technique assumes that no appreciable coalescence takes place between the impeller stream and discharge. In our tests, the apparent diameters are correlated by the expression

$$d_{vs} = 1.26\ \frac{d_I^{2/5}}{(Nd_I)^{6/5}} \cdot \left(\frac{d_T}{d_I}\right)^{6/5} \quad \text{(cgs. units)} \tag{10}$$

The standard deviation of the volume-surface diameter is 1.8 for $N_{Re_I} > 5 \times 10^4$. Equation (10) is consistent with expressions for the break-up of drops due to external velocity fluctuations whenever the scales of turbulence in the inertial subrange overlap the particle diameters (*8*). Moreover, for a highly turbulent flow field, it has been shown that coalescence-redispersion processes barely influence continuous-phase transfer (*2*). On the other hand, Schindler and Treybal (*17*) report from measured drop-size changes coalescence-redispersion frequencies of 0.2 to 2 min.^{-1} for impeller Reynolds numbers between 20,000 and 50,000 and a dispersed-phase volume fraction of 0.148. These frequencies are not much slower than our dispersed-phase residence times, which ranged from 0.1 to 0.5 min. Evidence (*7*) exists that much lower coalescence rates than those estimated by Schindler and Treybal pertain in systems of high interfacial tension, and the interfacial tension was almost an order higher in our tests, having a constant value of 50.4 dyne/cm. independent of solute mass flux. Moreover, the dispersed-phase volume fractions were at all times less than 0.148 (mostly of order 0.05 in our work), and it is known that coalescence rates fall off as the drop population becomes sparser (*13*). We thus conclude that the measured interfacial area adequately represents that within the mixer.

In extraction vessels, solute transfer occurs during the initial dispersion and the final coalescence of the dispersed phase. These unavoidable end-effects are not directly related to mass transfer promoted by turbulence within the mixing vessel; these effects are thus estimated separately and subtracted from the total solute transfer that is measured. The mass transferred from the undispersed iso-octane jet was calculated using a mass transfer coefficient based on penetration theory,

$$K_{Cj} = \sqrt{\frac{4\mathcal{D}}{\pi\theta_j}} \tag{11}$$

The contact time θ_j was estimated from the jet height and rise velocity. Transfer through the slowly moving interface in the settler was estimated from an expression obtained for a similar flow geometry (*14*):

$$N_{Sh_s} = 0.522\ N_{We}^{0.67} \left(\frac{\mu_C}{\mu_D}\right)^{0.254} N_{Sc}^{-1.46} \left(\frac{W_F G_C}{\mu_C}\right)^{0.397} \tag{12}$$

The second contribution to the outlet end-effect, that of transfer from entrained fine drops, is calculated from an expression (*18*) for transport under creeping-flow conditions:

$$N_{Sh_e} = 0.98\ N_{Re}^{1/3}\ N_{Sc}^{1/3} \tag{13}$$

This contribution, however, is negligible. The sum of these end-effects is very small, always less than 0.02 stage-efficiency equivalent, and is less than the errors introduced in the solute analyses. Unlike the more substantial end-effects found in solids dissolution (*5*), the low inlet-flow rates and the fast coalescence rates outside the mixer in our tests have led to insignificant end-effects. Not estimated is the very small solute transfer that occurred in the 0.5 to 1.5 sec. before the phases became substantially coalesced. Extrapolation of stage efficiencies to zero power input shows the calculated end-effects to be realistic (Figure 3).

TABLE 1. EXTRACTION-VESSEL DIMENSIONS USED IN TESTS

Vessel diam., m.	Vessel ht. m.	Vessel vol. 10^{-3} m.	Impeller diam. cm.	Blade width cm.	Diam. ratio d_T/d_I
0.1405	0.1437	2.090	4.49	0.561	3.13
0.1405	0.1437	2.090	7.26	0.894	1.94
0.1976	0.199	5.875	5.43	0.721	3.64
0.1976	0.199	5.875	7.26	0.894	2.72
0.1976	0.199	5.875	10.29	1.27	1.93
0.222	0.225	8.408	6.27	0.820	3.54
0.222	0.225	8.408	7.66	0.933	2.90
0.222	0.225	8.408	11.83	1.422	1.88

Likewise, the extraction that occurred in the sampling lines, where the transfer time was between 2 and 3 sec., was considered to be negligibly small compared with that in the vessel itself.

From Rosenweig's explicit expression (*16*) for the degree of unmixedness, the degree of mixing was between 92.5 and 98.8%. This result is supported by experimental observations (*1, 15*) for equipment of similar geometry to that used by us. Consequently it was assumed that the continuous phase was completely mixed. The dispersed phase may not, however, be completely mixed should internal circulation be weak or absent. Two limiting cases were considered: (a) when the dispersed phase is completely mixed, and the driving force everywhere is constant and equal to $(c_{C_2}^* - c_{C_2})$; (b) when the dispersed phase is unmixed, and the driving force is estimated by a step-by-step numerical analysis. The coefficients derived from these driving forces will be labelled K_C' and K_C'' respectively.

Plots of N'_{Sh_I} and of N''_{Sh_I} against N_{Re_I} are given in Figures 4 and 5. In each case, the data are compared with a line of slope 1.5, as predicted by Equation (5). The data cover a range of impeller Reynolds numbers from 14,250 to 94,100, and of Schmidt numbers from 1,463 to 1,644. Statistically the data for assumption of well-mixed drops regress with a Reynolds number exponent of 1.70, and for the case of unmixed drops the exponent becomes 1.36 with slightly less scatter of the data points. This value agrees with that of 1.375 predicted by Equation (7) which allows for the weak dependence of the drag coefficient on the impeller-tip speed. This dependence is also found in dissolution studies (*4*) for *o*-nitrophenol particles of volume-surface diameter 0.098 cm. agitated in the same vessel under similar hydrodynamic conditions

$$N'_{Sh_T} = 0.072\ N_{Re_I}^{0.81}\ N_{Sc}^{0.33} \qquad (14)$$

(for $10^4 < N_{Re_I} < 2 \times 10^5$). The anticipated exponent is 0.825 (*9*). The lesser influence of the impeller speed cannot be ascribed to the density differences for the systems; rather, the lack of surface mobility increases the extent of turbulence damping in the continuous-phase boundary layer.

A slight reduction in the scatter of the mass transfer data is obtained if the inclusion of vessel parameters is made

$$N''_{Sh_I} \sim d_I^{-0.86}\ (d_I/d_T)^{0.5} \qquad (15)$$

A term in $1/d_I$ is expected from the derivation of Equation (5), and the diameter ratio d_I/d_T may reflect the more intensive turbulence close to the walls with the proportionately larger impellers.

To summarize, the data resolve best as shown in Figure 6; this correlation includes the influence of vessel geometry and the mass transfer coefficients are based on the assumption of no mixing in the dispersed phase.

It is useful to compare and contrast our work with Schindler and Treybal's experiments. The vessel arrangements are similar, and so are the throughputs:

our data:
water flow 454 kg./h to 1,214 kg./h, $0.02 < \varphi_D < 0.11$
previous data:
total flow 670 kg./h to 900 kg./h, $\varphi_D = 0.145$

However, the systems themselves are very different. The binary system of the earlier work has an interfacial tension of 6.1 dyne/cm., whereas the ternary system of this work had an interfacial tension of 50.4 dyne/cm. In consequence, coalescence dispersion was fairly rapid in the former case, and much more sluggish in the latter. Nonetheless, the influence of impeller-tip speed on the continuous-phase mass transfer coefficient is similar. The exponent on the velocity term is 1.47 for 3 in. paddles and 1.50 for 5 in. paddles in the earlier tests. The coefficient K'_c for the two data sets, uncorrected for small changes in N_{Sc}, is plotted against power dissipation in Figure 7. The data sets merge into each other and cover a hundredfold range in power dissipation. Again, the influence of the various values

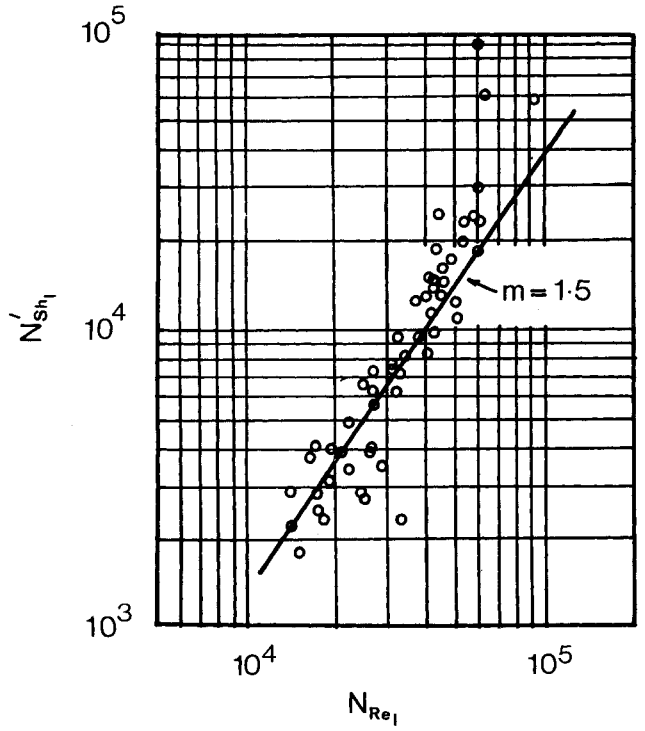

Fig. 4. Plot of impeller Sherwood number against impeller Reynolds number assuming dispersed phase to be completely mixed; continuous phase is also well mixed.

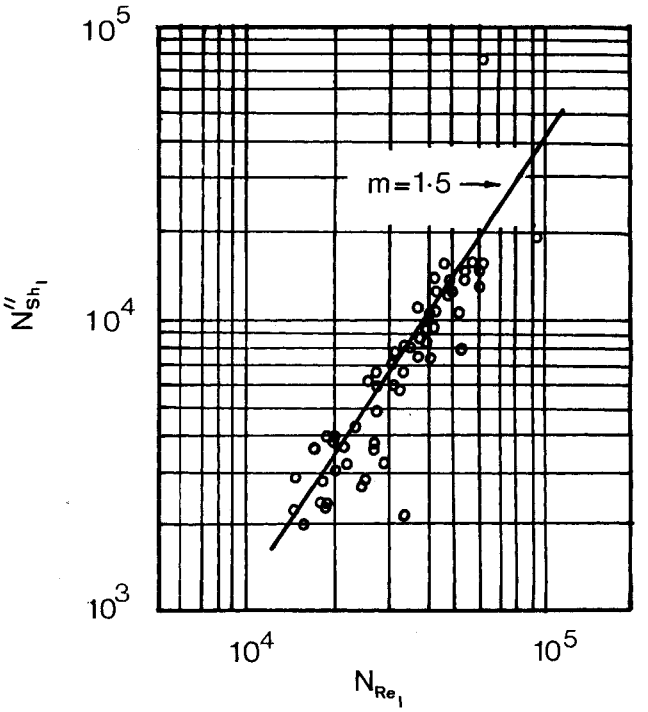

Fig. 5. As for Figure 4, but the driving force is based on assumption of an unmixed dispersed phase.

of tank and impeller diameters appears to be secondary for the geometries chosen. Power per unit tank volume is not a correlating variable.

CONCLUSIONS

The available data for area-free mass transfer coefficients for continuous-phase transport in mixers suggest that these coefficients correlate with the assumption that the particles are surrounded by a turbulent boundary layer. Dissolution of freely suspended solid particles correlate in a like manner, but the extent of turbulence damping appears to be greater. There is some evidence that the drag coefficient for the entrained particle varies with impeller-tip speed for impeller Reynolds numbers between 10^4 and 10^5. The data also show that the dimensional relationships, derived from the postulate of locally isotropic turbulence, may be useful in scaling mass transfer behavior from one set of conditions to another for impeller Reynolds numbers within this range.

ACKNOWLEDGMENT

The authors acknowledge financial assistance from the New Zealand University Grants Committee (Grant 62/169) and from the Council of the University of Canterbury. J. B. Glen received an award of a University Grants Committee Fellowship to carry out the work.

NOTATION

$\overline{a_i}$ = mean interfacial area, $(L)^{-1}$
b = a coefficient, defined in Equation (1)
c_C = continuous-phase concentration of solute, $(M)(L)^{-3}$

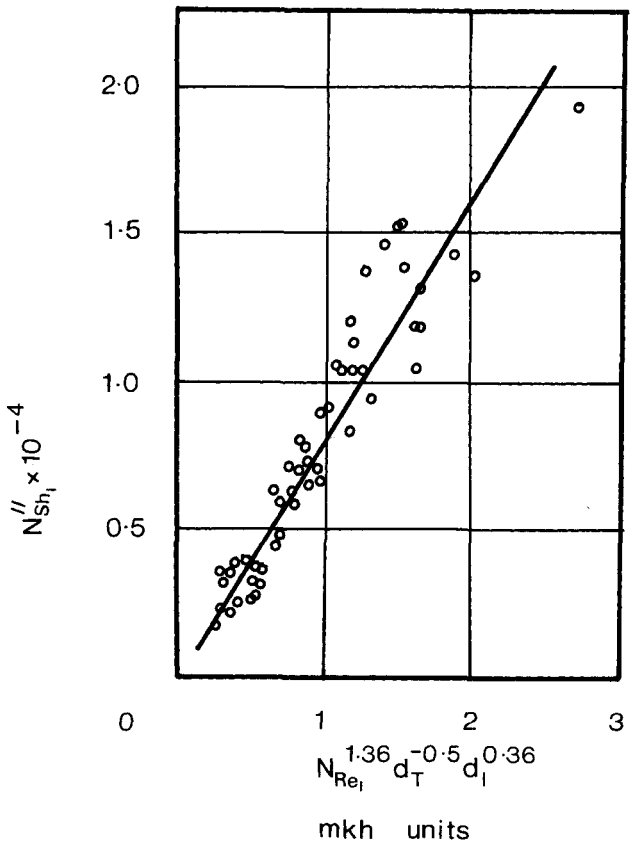

Fig. 6. General correlation of all data. Equation of line is $N''_{SHI} = 8.92 \times 10^{-4}\ N_{ReI}^{1.36}\ {}_{dT}{}^{-0.5}\ {}_{dI}{}^{-0.36}$ —338, mkh units. Regression coefficient is 0.931.

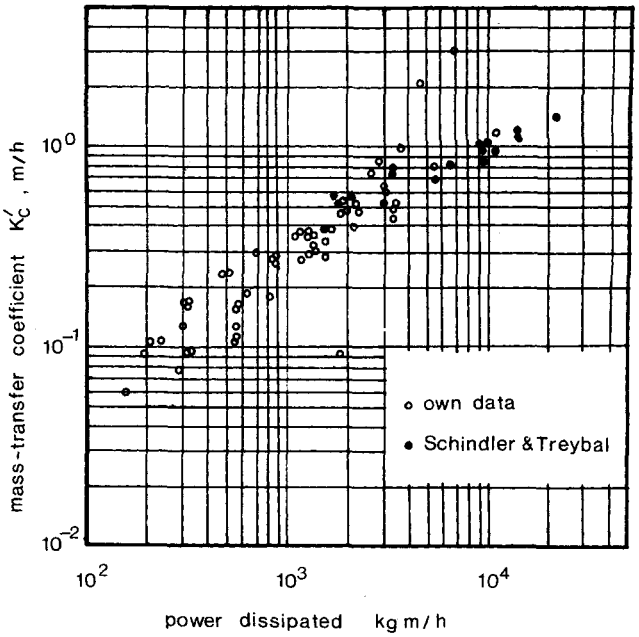

Fig. 7. Plot of mass transfer coefficient (well-mixed drops) against power dissipation in mixing; graph is uncorrected for small changes in N_{Sc}.

c_D = dispersed-phase concentration of solute, $(M)(L)^{-3}$
C_{DF} = skin-friction drag coefficient
d_I = impeller diameter, (L)
dp = particle diameter, (L)
d_{vs} = tank diameter, (L)
d_T = volume-surface mean diameter, (L)
$\mathcal{D}$ = diffusivity, $(L)^2(T)^{-1}$
G_C = specific mass flow of continuous phase, $(M)(L)^{-2}(T)^{-1}$
K_C = continuous-phase mass transfer coefficient, $(L)(T)^{-1}$
N = impeller rotational speed, $(T)^{-1}$
P = power dissipation, $(M)(L)^2(T)^{-3}$
Q_C = continuous-phase flow rate, $(L)^3(T)^{-1}$
U = slip velocity between particle and stream, $(L)(T)^{-1}$
W_F = flow sectional width in settler, (L)

Greek Letters

ϵ = energy dissipation, $(M)(L)^{-1}(T)^{-3}$
μ_C = continuous-phase viscosity, $(M)(L)^{-1}(T)^{-1}$
μ_D = dispersed-phase viscosity, $(M)(L)^{-1}(T)^{-1}$
ν_C = continuous-phase kinematic viscosity, $(L)^2(T)^{-1}$
ν_{turb} = turbulent kinematic viscosity, $(L)^2(T)^{-1}$
ρ_C = continuous-phase density, $(M)(L)^{-3}$
ρ_D = dispersed-phase density, $(M)(L)^{-3}$
$\Delta\rho$ = density difference $(\rho_C - \rho_D)$, $(M)(L)^{-3}$
σ = surface tension, $(M)(T)^{-2}$
θ_j = jet contact time, (T)

Dimensionless Groups

N_{ReI} = impeller Reynolds number, Nd_I^2/ν_C
N_{Sc} = Schmidt number, $\nu_C/\mathcal{D}$
N'_{ShI} = Sherwood number, $\overline{K_C}'d_I/\mathcal{D}$
$N''_{ShI} = \overline{K_C}''d_I/\mathcal{D}$
$N'_{ShT} = \overline{K_C}'d_T/\mathcal{D}$
N_{We} = Weber number, $\rho U^2 W_F/\sigma$

Superscripts

* = equilibrium value
$'$ = totally mixed dispersed phase

$''$ = unmixed dispersed phase
$-$ = time-smoothed value

LITERATURE CITED

1. Biggs, R. D., *AIChE J.*, **9**, 636 (1963).
2. Boyadzhier, L., and D. Elenkov, *Chem. Eng. Sci.*, **21**, 955 (1966).
3. Buraway, A., and J. T. Chamberlain, *J. Chem. Soc.*, **155**, 2310, 3734 (1952).
4. Dobbie, T. P., *B. E. Report, Univ. Canterbury*, Christchurch, New Zealand (1964).
5. Flynn, A. W., and R. E. Treybal, *AIChE J.*, **1**, 324 (1955).
6. Glen, J. B., *Ph.D. thesis, Univ. Canterbury*, Christchurch, New Zealand (1965).
7. Hillestad, J. G., and J. H. Rushton, Paper presented to AIChE Meeting, Columbus, Ohio (May, 1966).
8. Hinze, J. O., *AIChE J.*, **1**, 289 (1955).
9. Keey, R. B., and J. B. Glen, *Can. J. Chem. Eng.*, **42**, 227 (1964).
10. ———, *Brit. Chem. Eng.*, **12**, 1081 (1967).
11. Levich, V. G., "Physicochemical Hydrodynamics," Prentice-Hall, Englewood Cliffs, N. J. (1962).
12. Lin, C. C., R. Moulton and G. Putnam, *Ind. Eng. Chem.*, **45**, 636 (1953).
13. Madden, A. J., and G. L. Damerall, *AIChE J.*, **8**, 233 (1962).
14. Murphy, N. F., T. E. Lastovica, and A. E. Skrzee, *ibid.*, **2**, 451 (1956).
15. Rice, A. W., H. L. Toor, and F. S. Manning, *ibid.*, **10**, 125 (1964).
16. Rosenweig, R. E., *ibid.*, **10**, 91 (1964).
17. Schindler, H. D., and R. E. Treybal, *ibid.*, **12**, 790 (1968).
18. Ward, D. M., O. Trass, and A. J. Johnson, *Can. J. Chem. Eng.*, **40**, 164 (1962).

The Reduction in Heat Exchanger Effectiveness Caused by Dilute Quantities of Drag Reducing Substances

D. A. WHITE

University College London, London, England

In a recent communication (*1*) K. A. Smith and others have published further data on heat transfer to drag-reducing polymer systems. These systems have received considerable study because there is clearly some practical advantage in using additives to cut down pumping requirements. In a recent study (*2*) I have pointed out the possibility that use of these additives in tube heat exchangers may have no beneficial effect whatsoever. It is gratifying to see that Smith's results also confirm this trend.

Their turbulent flow heat transfer data for dilute polymer solutions has been correlated in a form easily amenable for design purposes. Rearranging their equation (5) one obtains

$$h = \frac{\tau}{U} \cdot \frac{c_p^{0.4} k^{0.6}}{\mu^{0.6}} \qquad (1)$$

or, assuming that physical properties are unaffected by addition of small amounts of polymer

$$h = \text{const.} \times \frac{\tau}{U} \qquad (2)$$

For the effect of drag reduction to have practical application the addition of polymer must ensure that the heat transfer coefficient divided by pumping power is increased. Pumping power is proportional to $\tau\ U$. Hence the important ratio is $h/\tau\ U$. From Equation (2), we may write

$$\frac{h}{\tau\ U} \sim \frac{1}{U^2}$$

for a given τ, U is increased by addition of polymer so $h/\tau U$ is decreased. Again the Toms effect appears to offer no practical benefit in high Reynolds number heat transfer in a smooth pipe. In retrospect this is not surprising since turbulence promoters are often used in process heat exchangers. Here a higher wall shear stress is accepted as necessary to cut down the thickness of the laminar sublayer, it being of the greater importance to cut down the thickness of this layer than to decrease wall shear stress. In contrast the laminar sublayer is thickened by dilute polymer solutions under drag reducing conditions.

It should also be pointed out that reasonable correlations have been obtained by several workers (*1*, *3* to *5*) using straightforward modifications of turbulent flow heat transfer analogies (*6*). All this type of work requires *a priori* knowledge of turbulent flow friction factor data for the given system. In so far as very little satisfactory work has been done on the friction correlation problem the calculation of heat transfer data for turbulent flow of dilute polymer solutions remains unsolved. For this reason the latter problem is probably a more important area of research.

NOTATION

c_p = heat capacity of solution, $(L^2T^{-2}\theta^{-1})$
h = heat transfer coefficient for the pipe, $(M\ T^{-3}\theta^{-1})$
k = thermal conductivity of solution, $(MLT^{-3}\theta^{-1})$
U = mean velocity, (LT^{-1})
μ = solution viscosity, $(ML^{-1}T^{-1})$
τ = pipe wall shear stress, $(ML^{-1}T^{-2})$
(M = mass, L = length, T = time and θ = temperature units)

LITERATURE CITED

1. Smith, K. A., et al., *AIChE J.*, **15**, 294 (1969).
2. White, D. A., *Chem. Eng. Sci.*, **24**, 911 (1969).
3. Wells, C. S., *AIChE J.*, **14**, 406 (1968).
4. Gupta, K., et al., *Int. J. Heat Mass Transfer*, **10**, 1211 (1967).
5. Poreh, M., et al., *ibid.*, **11**, 805 (1968).
6. Levich, V. G., "Physicochemical Hydrodynamics," p. 171, Prentice Hall, Englewood Cliffs, N. J. Prentice Hall, (1962).